南京航空航天大学

论文集

（二〇〇二年）

第2册

一院

南京航空航天大学科技部编

二〇〇三年六月

一　　院

○一二系

序号	姓　名	职称	单位	论文题目	刊物、会议名称	年、卷、期	类别
1	陈红全	正高	012	隐式无网格算法及其应用研究	空气动力学学报	2002.20.02	J
2	陈红全 黄明恪	正高 正高	012 012	气动外形表面雷达吸波涂层问题电磁散射场的数值模拟	计算物理	2002.19.06	H
3	程克明 吕英伟 张其威	正高 中级 正高	012 012 012	侧向喷流的一种直接实验模拟	流体力学实验与测量	2002.16.02	J
4	程克明	正高	012	背风涡隔离对大攻角旋成体表面压力分布的影响	南京航空航天大学学报	2002.34.02	J
5	程克明	正高	012	大攻角流动非对称性成因与对策	南京航空航天大学学报	2002.34.01	J
6	程克明 伍贻兆 吕英伟	正高 正高 中级	012 012 012	侧向喷流试验中干扰力和喷流力同时模拟的相容性	南京航空航天大学学报	2002.34.06	J
7	顾蕴松 明晓	中级 正高	012 012	舰船飞行甲板真实流场特性试验研究	航空学报	2002.22.06	H
8	顾蕴松 明晓	中级 正高	012 012	表面热膜在高超声速边界层中的应用	宇航学报	2001.22.16	H
9	黄明恪 陈红全	正高 正高	012 012	用非结构网格和欧拉方程计算运载火箭绕流	宇航学报	2002.23.05	H
10	黄明恪 陈红全	正高 正高	012 012	非结构直角网络用于复杂外形	第十一届全国计算流体力学会议	2002.01	
11	黄明恪	正高	012	用非结构直角网格和欧拉方程计算飞机绕流	航空学报	2002.23.06	H
12	李甘牛 明晓	中级 正高	012 012	双谱分析在流体非线性力学中的应用	数据采集与处理	2002.17.01	H
13	李甘牛 明晓	中级 正高	012 012	射流边界中基波与亚谐波相互作用的实验研究	空气动力学学报	2001.19.04	J*
14	李甘牛 明晓	中级 正高	012 012	射流撞击折板的实验研究	南京航空航天大学学报	2002.34.04	J
15	刘学强 伍贻兆 夏健	中级 正高 副高	012 012 012	多重网格在非结构网格中的应用	计算物理	2002.19.04	H
16	刘学强 伍贻兆 夏健	中级 正高 副高	012 012 012	用混合网格及各项异性变型网格法求解三维可压紊流流动	应用力学学报	2002.19.03	J
17	刘学强 伍贻兆 夏健	中级 正高 副高	012 012 012	用混合网格求解三维可压雷诺平均N-S方程	计算力学学报	2002.19.03	H
18	刘学强 伍贻兆	中级 正高	012 012	用基于混合网格的多重网格数值模拟绕物体的紊流动	宇航学报	2002.23.04	H
19	吕宏强 伍贻兆 夏健	博士 正高 中级	012 012 012	非结构聚合多重网格法数值模拟研究	航空学报	2002.23.01	H

序号	姓 名	职称	单位	论文题目	刊物、会议名称	年、卷、期	类别
20	沈宏良 刘昶	中级 正高	012 012	Investigation of flight dynamics of thrust vectoring aircraft using extend continuation methods	南京航空航天大学（英文版）	2002.19.02	J
21	沈宏良 曹万里 刘昶	中级 硕士 正高	012 012 012	飞行横向敏捷性的优化计算	飞行力学	2002.20.01	J
22	史志伟 吴根兴	中级 正高	012 012	多变量非线性非定常气动力的模糊逻辑模型	空气动力学学报	2002.19.01	J
23	隋洪涛 陈红全 黄明恪	博士 正高 正高	012 012 012	Pareto 基因算法多目标翼型优化设计	航空学报	2002.23.02	H
24	唐登斌 夏浩	正高 硕士	012 012	Nonlinear Evolution Analysis of T-S Disturbance Wave at Finite Amplitude in Nonparallel Boundary Layers	Applied Mathematics and Mechanics	2002.23.06	SCI、EI、W
25	唐登斌	正高	012	孤帆一片日边来	力学与实践	2002.24.06	H
26	唐登斌	正高	012	可压缩流非平行边界层稳定性研究	航空学报	2002.23.02	EI、H
27	田春 张强 谷嘉锦	博士 副高 正高	012 012 012	横流风机流场与声场综合研究用装置的研制	噪声与振动控制	2002.22.01	J
28	田春 张强	博士 副高	012 012	流动诱导空腔震荡预测方法的改进	南京航空航天大学学报	2002.34.02	J
29	王江峰 伍贻兆	中级 正高	012 012	Genetic Algorithms and Game Theory for the High-lift Design Problem in Aerodynamics	南京航空航天大学学报（英文版）	2002.19.01	J
30	王江峰 伍贻兆	中级 正高	012 012	二维横向喷流与超音速主流干扰流场的N-S方程数值解	南京理工大学学报	2002.126.06	J
31	王江峰	中级	012	研究生教学与培养的思考	南京航空航天大学学报（社科版）	2002.04.00	
32	王伟志 唐登斌	博士 正高	012 012	边界层稳定性的外平行性问题研究	南京航空航天大学学报	2002.34.04	J
33	王伟志 唐登斌	博士 正高	012 012	Falkner_skan流空间演化的二次稳定性研究	空气动力学学报	2002.20.04	J
34	王伟志 唐登斌	博士 正高	012 012	Effects of Nonparallelism on the Boundary Layer Stability	Journal of Hydrodynamics	2002.14.04	J
35	夏浩 唐登斌	硕士 正高	012 012	三维扰动的非平行稳定性研究	力学学报	2002.34.05	H

序号	姓 名	职 称	单位	论 文 题 目	刊物、会议名称	年、卷、期	类别
36	夏浩 唐登斌	硕士 正高	012 012	A Detailed Non-Parallel Stability Analysis Using Paranolic Stability Equation	Computational Fluid Dynamics Journal (Japan)	2002.10.04	W
37	杨屹生	正高	012	Finite Element Method for the Transient Process of the Seperation of External Stores from Aircraft	CHINESE JOURNAL OF AERONAUTICS	2002.15.01	H
38	姚裕 吴洪涛 张召明	初级 正高 副高	012 053 012	基于Stewart平台的六维力传感器在风洞天平中的应用	淮海工学院学报	2002.11.04	
39	张立 唐登斌	博士 正高	012 012	槽道湍流相干结构的研究	南京航空航天大学学报	2002.34.06	J
40	张强 王华明 胡章伟	副高 副高 正高	012 011 012	Wavelet analysis of helicopter noise signal	声学学报（英文版）	2002.21.01	H
41	张召明 李京伯	副高 正高	012 012	CAARC高层建筑标模动态测力研究	南京航空航天大学学报	2002.34.03	J
42	张召明	副高	012	南航风工程研究简介	第六届全国风工程及工业空气动力学学术会议	2002.01	
43	赵宁 余彦	正高 硕士	012 012	R-M不稳定性数值模拟方法	计算数学	2001.23.04	H*
44	赵熙强	博士后	012	The Algebraic Properties of a Type of Infinite Lover Triangular Matries Related to Derivatives	数学研究与评论	2002.22.04	H
45	赵熙强	博士后	012	Sequence Related to Riordem Arrays	The Fibonacci Quarterty	2002.40.03	SCI、W
46	赵熙强 唐登斌	博士后 正高	012 012	A new note on a homogenous balance method	Physics Letter A	2002.297.00	SCI、W

Wavelet analysis of helicopter noise signal

ZHANG Qiang WANG Huaming HU Zhangwei

(*Department of Aerodynamics, Nanjing University of Aeronautics and Astronautics* Nanjing 210016)

Received Sept. 12, 2000

Revised Feb. 16, 2001

Abstract Helicopter noise features under typical flight condition were investigated based on wavelet transform. The contribution of blade-vortex interaction (BVI) to helicopter noise and low frequency oscillations beat was shown clearly from the detail of wavelet decomposition for helicopter noise signal.

PACS numbers: 43.28, 43.60

1 Introduction

At the present time, for civil helicopters, stronger limitation is imposed by certification rules to reduce acoustic nuisance. And for military helicopters, noise reduction has also been concerned in limitation of detectability. Therefore helicopter noise generation and control has become an increasingly important problem for the helicopter design. For turbine-driven helicopter widely used at present, the noise generation mechanism can be divided into aerodynamic noise and machinery noise. The aerodynamic noise is due to the rotation of rotor blades and jet. The machinery noise comes from speed reducer and power transmission of the engine. For far-field noise, the aerodynamic noise is dominant contributor of helicopter noise and its spectra are composed of discrete frequency components and broad band components. These discrete noise and broad band noise are produced respectively by periodic aerodynamic forces (steady or unsteady) and random aerodynamic pressure fluctuation acting on rotating rotor blades. Measurement shows the discrete noise is main noise source. Therefore the research effort in the present is concentrated on the discrete noise, in particular blade-vortex interaction (BVI) noise and high-speed impulsive noise[1,2]. Due to pitch control, flapping, lagging and BVI, main rotor operates in a serious unsteady aerodynamic environment so that its noise generation mechanism is very complex. For tail rotor, its generation mechanism is even more complex because it is in wake of the main rotor. To further understand the mechanism of helicopter noise, researchers have devoted much attention to newly developed signal distinguishing technique. In this paper, the wavelet analysis technique is applied to extract the main components of helicopter noise. The results prove this technique is helpful on the understanding the mechanism of helicopter noise.

2 Helicopter noise signal analysis based on wavelet transform

2.1 A brief introduction to wavelet transform

Wavelet analysis is a new time-frequency analysis method. Wavelet transform is defined as[3,4]

$$Wf(t,s) = \frac{1}{\sqrt{s}} \int_{-\infty}^{\infty} f(\tau)\psi\left(\frac{\tau - t}{s}\right) \mathrm{d}\tau.$$

In the equation the frequency parameter f is replaced by scale parameter s. Therefore the wavelet transform is referred to a time-scale plane rather than a time-frequency plane. On the scale axis the small-scale corresponds to the high frequency region and the large-scale corresponds to the low frequency region. A characteristic of the wavelet transform lies in the introduction of an adaptive band pass window $(\psi((\tau - t)/s))$. The high frequency region of the signal (i.e. small- scale value of s) corresponds to short time window and the low frequency region of the signal(i.e. large-scale value of s) corresponds to long time window. This is the reason why using wavelet transform not only the components of short time-high frequency in the signal are analyzed efficiently but also the low frequency-slow varying components in the signal are estimated accurately. In addition, based on wavelet analysis the signal is not only decomposed into a series of details of wavelet decomposition, but also several details which are arbitrarily extracted from the series details can be reconstructed into a new signal. It is very useful for the noise mechanism study. It is the reason the wavelet analysis was used in this paper. For discrete wavelet transform, the signal is decomposed into a detail component (Wf) and an approach component (Sf) of wavelet decomposition on every step. For example, when sampling frequency is 1380 Hz the octave coverage region of details and approach of wavelet decomposition in frequency domain are represented in Fig. 1.

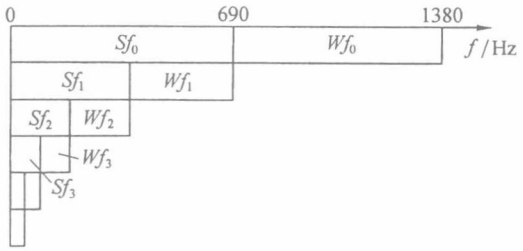

Fig. 1 Process of decomposing signal into a series of details and an approach components step by step

2.2 Flight measurement of helicopter noise

Flight noise of Ecureuil AS350B2 Helicopter was measured in this paper. The noise data and helicopter position corresponding to various typical flight conditions were stored into data-bank. The arrangement of noise measurement is represented in Fig. 2. Flight conditions of the helicopter are comprised of 9° - climb, maximum continuous power climb, level flight, 4°, 6°, 8° and 10° - descent. Flight velocities are comprised of 70 km/h, 102 km/h, 140 km/h and 220 km/h. Actual flight state of helicopter was obtained by flight track homing system.

For the far field measurement, in order to avoid the sound interference from ground reflection in the low-mid frequency range the ground microphone is placed upside down and point to an aluminum plate that is 400mm in diameter. The aluminum plates are flushed mounted on the ground surface and keep 7mm distance from the microphones. Three cameras with a scale mark are placed under the flight track (see Fig. 2). When helicopter flies over these cameras, its picture will be taken, and the camera pulse signals are simultaneously sent to FM tape recorder (used for recording noise signals). By using this special technique the helicopter flight position above these cameras (flight altitude and yawing distance) are provided. But flight track (including flight velocities) is recorded with a vision tracker. Atmosphere parameters (including wind velocity and direction, temperature, moisture, atmosphere pressure) are provided by atmosphere station of airport. The equipment on the helicopter are mainly used to record flight parameters, rotational impulsive signals of main and tail rotor as well as helicopter noise signals from two nose cone microphones, which are mounted at left sled and right horizontal tail wing.

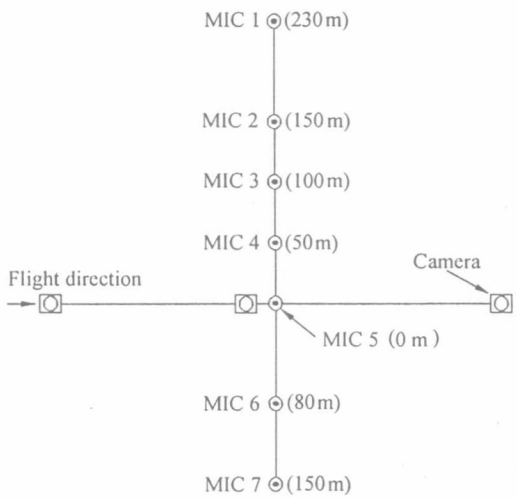

Fig. 2 The arrangement of noise measurement points

2.3 Extracting and analysis of helicopter noise feature

It is found on the basis of the helicopter noise measurement that a strong periodic spikes appear in the sound pressure time histories of the helicopter ground noise when helicopter descends at $6° - 10°$ with a mid-low speed (see Fig. 4). The appearance of the spikes is caused by very strong local unsteady aerodynamic force on the main rotor, which is due to blade and vortex interaction (BVI). In the following part of this paper, the BVI impulsive noise will be analyzed by using wavelet analysis technique.

It is known from wavelet analysis theory that the helicopter noise signal can be decomposed into wavelet details corresponding to different frequency band so that those undistinguished features become distinct in subspace of different frequency band (i.e. form wavelet detail), whereas wavelets corresponding to a specific time in the details can be selected to reconstruct a interesting sound signal (i.e. the feature of the helicopter noise is extracted based on inverse

wavelet transform). Here, as an example, the ground noise signals respect to three positions of the helicopter at the 8° -descent (flight velocity, 102 km/h) were analyzed and discussed. The three positions are shown in Fig. 3. Fig. 4 represents the sound pressure time histories of original signal and reconstructed signal, here, for the reconstructed signal the BVI spikes were excluded. It is found from the sound pressure time histories of original signal that the period of the spikes in sound pressure time histories is identified with the rotational cycle of the main rotor. It demonstrates that BVI impulsive noise happens on above flight condition. It should point out that the impulsive noise also appears in high-speed flight, but on above flight condition the advancing blade tip speed (Mach number, about 0.76) is not high enough to produce high-speed impulsive noise. In order to quantify the influence of BVI the wavelet analysis technique was used in this paper. The details of wavelet decomposition at main measurement point are

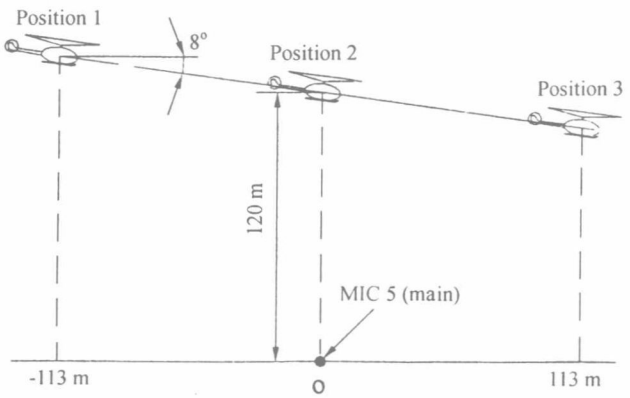

Fig. 3 Three positions of the helicopter corresponding to main measurement point

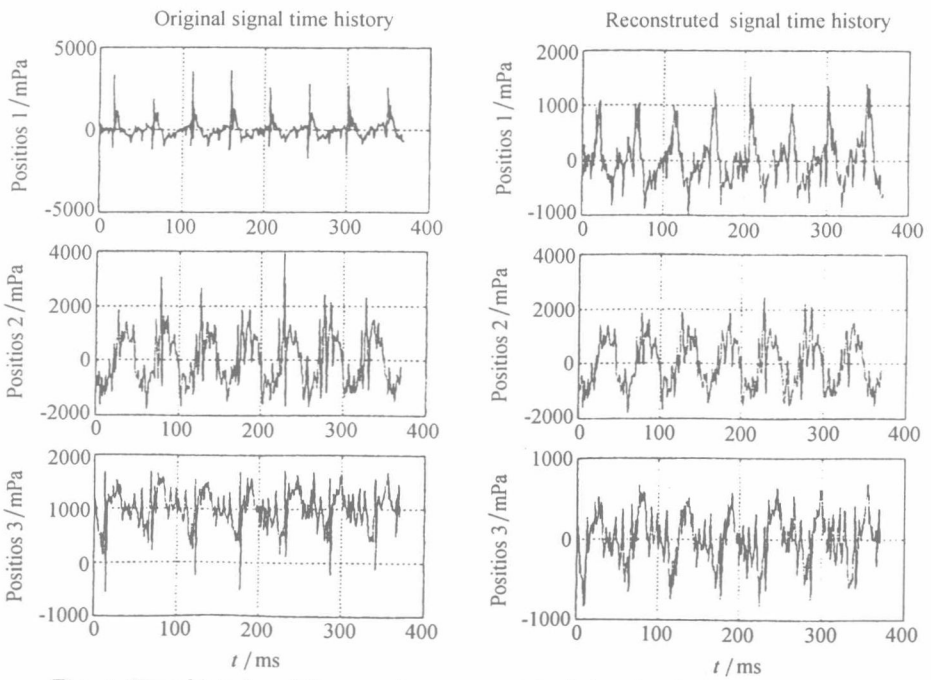

Fig. 4 Time histories of the sound pressure original signal and reconstructed signal

shown in Fig. 5. The A-weighted spectra, both for original signal and reconstructed signal (excluded BVI spikes) at main measurement point are shown Fig. 6. A-weighted sound pressure levels of total noise and its BVI component are shown in Table 1.

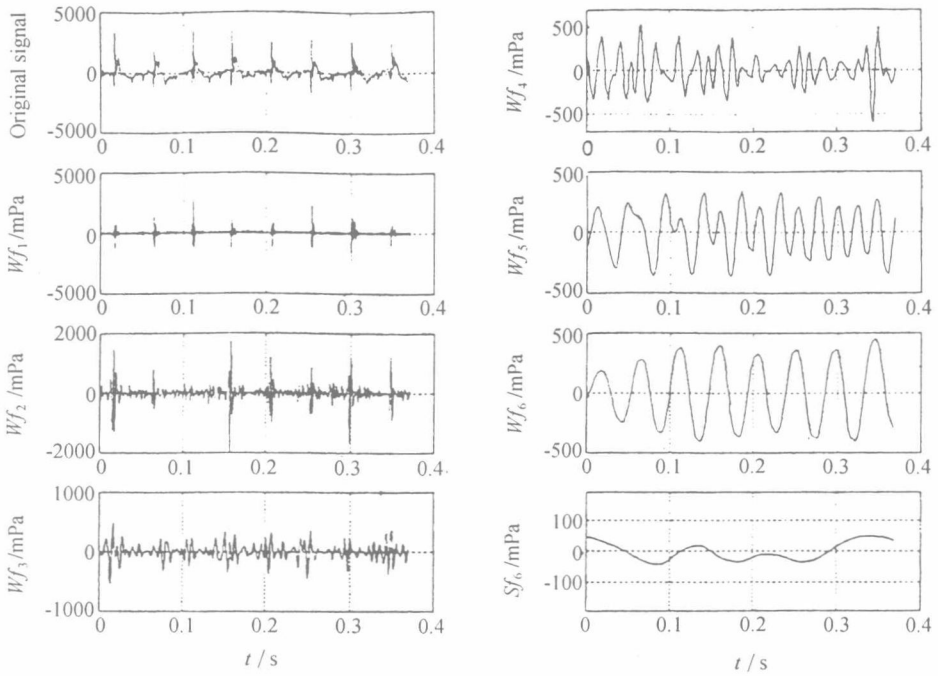

Fig. 5 Details of wavelet decomposition

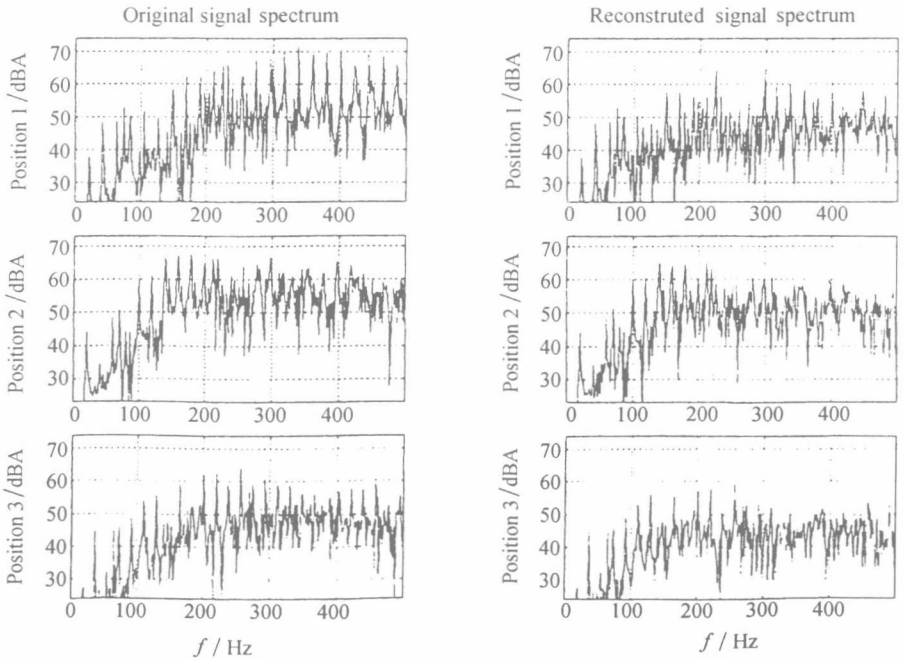

Fig. 6 A-weighted spectra of original signal and reconstructed signal

Table. 1 A-weighted sound pressure levels of total noise and its BVI component (dBA)

Measurement points	Position 1		Position 2		Position 3	
	Total	BVI	Total	BVI	Total	BVI
Point 2	76.6	75.3	76.4	73.1	75.6	73.0
Point 5	84.1	83.4	83.2	80.4	76.3	73.9
Point 7	73.2	70.0	73.5	69.6	69.2	65.2

Discussion on the results of wavelet analysis at 8° (102 km/h)-descent condition:

(1) Table 1 shows variation of BVI noise component with the helicopter position, which indicates strong directivity of BVI impulsive noise. It is found that the BVI noise component is not easy to distinguish in the sound pressure time history when it is weaker comparing to the remainder (without BVI noise component). Therefore application of the wavelet analysis technique to extract the BVI impulsive signal is helpful to obtaining a better results. The BVI spike and the instant of its occurrence can be clearly seen in detail components Wf1 and Wf2 of Fig. 5. Obviously for extracted feature of helicopter noise signal the wavelet analysis has a function of the "numerical microscope", while the pure time-domain or frequency-domain analysis do not possess this function.

(2) For the analysis of BVI features, first, wavelets corresponding to spikes were extracted from wavelet details Wf1, Wf2 in Fig. 5 and added together to reconstruct a new signal (i.e. BVI impulsive noise). For BVI impulsive noise, its amplitude, width, period and occurrence instant in a rotary period of the rotor describe its features. The directivity of BVI impulsive noise may be obtained from flight track data corresponding to measurement point and the SPL of the reconstructed signal of BVI. Fig. 4 shows that BVI impulses (positive impulse) corresponding to the helicopter position 1, which are mainly caused due to the advancing blade, are stronger than those corresponding to the helicopter position 2. Fig. 4 also shows that BVI impulses corresponding to the helicopter position 3 are negative impulses, which are mainly caused due to the retreating blade. Furthermore, Table 1 shows that the BVI impulsive noise level at measurement point 7 is lower than that at measurement point 2, which indicates that the noise level in the advancing blade side is still higher than that in the retreating blade side even when the BVI impulsive noise is mainly produced by retreating blade.

(3) The difference between the reconstructed signal (right side in Fig. 6) and the original noise signal (left side in Fig. 6) shows that appearance of BVI enhances the high order harmonic components of main rotor blade passing frequency (about 20 Hz) and do not affect the harmonic components of tail rotor blade passing frequency (about 70 Hz), which indicates the BVI noise comes from the main rotor. In addition, the high order harmonic components enhanced by BVI are in the sensitive frequency range of human ear. For example, when the helicopter is in position 1 (see Table 1), the BVI noise level measured by the main measurement point is 83.4 dBA, while the total noise level of the helicopter is only 84.1 dBA. This means that BVI noise is effective noise source although it is a very narrow impulsive noise.

(4)A low frequency oscillation beat of the helicopter noise is shown from wavelet detail components Wf4 – Wf6 in Fig. 5. And its character varies with positions 1, 2 and 3. This can not be observed by only pure time-domain or frequency-domain analysis method.

3 Conclusions

The following conclusions are drawn from the wavelet analysis for the helicopter noise signal:

(1) Helicopter noise is different from propeller aircraft noise. Its frequency-domain spectra are more complex. In noise spectra, the amplitudes of higher harmonic components of helicopter blade passing frequency are decayed much slower with increasing of its order than that of propeller. It is the reason why helicopter noise, especially BVI noise produced by a helicopter descending with a middle or low speed, makes people nuisance.

(2) It is helpful to using wavelet technique to extract some helicopter noise features for analyzing helicopter noise mechanism.

(3) The results are encouraging though the analysis for helicopter noise signals based on wavelet transform in this paper is only a try.

References

[1] Hanno Heller. Helinoise—The european community rotor acoustics research program. AIAA 93–4358

[2] YAO Qihang *et al.* Aircraft Noise Engineering. Publishing House of Northwestern Polytechnical University , 1998

[3] Mallat S G. Zero–crossings of a wavelet transform. *IEEE Trans, Inform, Theory*, 1991; **37**(4): 1019—1033

[4] Stephance G Mallat. A theory for multiresolution signal decomposition. The wavelet representation. *IEEE Trans, ASSP*, 1989; **11**(7): 674—693

文章编号:1006—1355(2002)01—0024—03

横流风机流场与声场综合研究用装置的研制

田　春,张　强,谷嘉锦
(南京航空航天大学,南京 210016)

摘　要:基于国内外空调器横流风机流场与声场的有关标准,本文最新研制了用以优化和评价空调器横流风机性能的流场显示装置和流量、噪声同步实验装置,并阐明了它们设计中的考虑及其用途。

关键词:横流风机;流场显示;噪声测量
中图分类号:TB535　　**文献标识码**:A

Development of the device used for crossflow fan's fluid and Sound field

TIAN Chun, *ZHANG Qiang*, *GU Jia-jin*
(Nanjing University of Aeronautics and Astronautics, Nanjing 210016, China)

Abstract: Based on the norms for fluid field and sound field of air conditioner this paper developed the fluid field display device and fluid and sound synchronizing pilot plant which are built to optimize and assess the air conditioner product with crossflow fan. The use of them and design essential are stated on this paper.

Key words: crossflow fan; fluid field display; noise mersurement

引言

随着对空调器噪声的限制,使得横流风机流动噪声的研究变得越来越重要,但考虑到这类噪声研究的复杂性(既要使噪声降低又要保证其流动性能),因此有必要对空调器横流风机的流场和声场进行综合的研究。目前,国外已有相应的试验装置用于这方面的研究。鉴于国内对空调器的自行设计才刚起步,有必要研制一种经济实用的用于流场显示和流量、噪声同步实验装置。本文所研制的流场显示装置可通过观察烟谱图来研究横流风机系统流场的旋涡方式和流动情况,并采用横流风机流量、噪声同步实验装置同步测量横流风机在给定转速下的流量、压力、所耗功率、效率及其相应的噪声声压级等有关参数,从而达到对空调器产品进行优化设计和对其成品进行评估的目的。

1　空调器横流风机模型简介

横流风机模型是用于研究其通风性能及其噪声水平的试件。根据研究的需要常选用三类横流风机模型即二元模型、三元模型和成品原型。二元模型是指其贯穿风轮的流场为二元流场并是一种供风轮横截面方向流场显示用的模型。它是取自横流风机横截面方向的一片实体,包括叶轮、蜗舌和蜗壳,省略了其他部件,其中蜗壳的形状、叶轮和蜗舌的间距可以改变,目的是找出流场与声场品质比较好的最佳蜗壳线型。三元模型是指其贯穿风轮的流场为三元流场,并与二元模型相同,在实验过程中通过改变叶轮同蜗舌的间距及蜗壳的外型寻找在某给定流量下的通风性能和噪声水平较为合适的最优结构参数。成品原型将在横流风机流量、噪声同步实验装置中进行标定。

2　流场显示装置的研制

流场显示装置是横流风机流场和声场综合研究用的实验装置。它的主要功能是用于观察横流风机各种结构参数下所对应的贯穿整个风轮的烟谱图(结构参数可通过改变蜗壳外型、风轮与蜗舌的间距等来调节),从而达到在理论设计的基础上优化横流风机结构参数的目的。为了便于流场显示,该装置选用横流风机的二元模型作为其流场和声场综合研究的对象,并将其与装置本体和发烟系统安装在同一体中,参见图 1。

收稿日期:2001—03—16
作者简介:田春(1977－),女,硕士研究生。

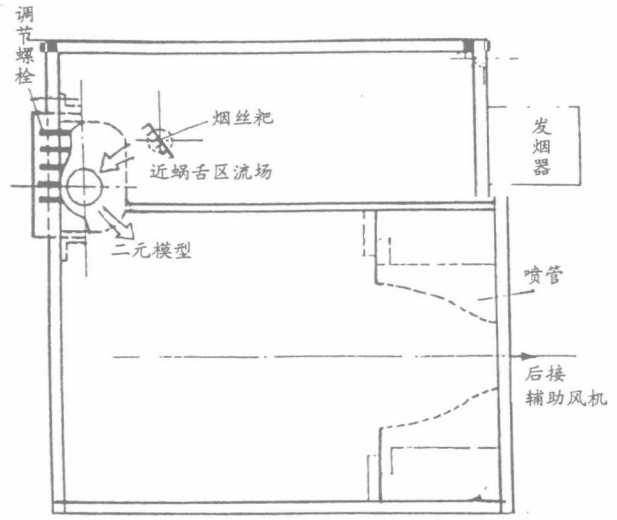

图 1 流场显示装置

关于流场显示装置研制中的关键技术问题有如下几点：

1）二元模型的流道宽度的选择。它应根据横流风轮叶栅结构来定，一般对叶栅结构在轴向变化较大的横流风轮来说应选择较小的流道宽度，这样才能作为二元模型，否则将作三元模型处理。

2）蜗壳线型的调节。为了操作方便选用了有弹性的不锈钢薄片作为蜗壳型面其蜗壳的基准曲线是由生产厂家提供的理论设计蜗壳曲线，在此基础上，可通过调节螺杆来改变蜗壳的线型。

3）蜗舌与风轮的间距的调节。由于叶片尾迹的存在，非常接近于叶轮出口处的周向速度分布呈现出最大、最小值。在这一区域放置蜗舌将产生强的压力脉动，因而形成了叶片通过频率和其谐波的有效声辐射。而且蜗舌接近叶轮将周期性地阻塞两叶片间的流动。不稳定的流动建立起不稳定的叶片力，这种力是叶轮产生离散噪声的一个原因。通过调节蜗舌与风轮的间距，观察蜗舌区的烟谱图，运用涡声理论来找出合适的间距[1]。

4）发烟器的选用。除考虑到横流风机系统易受酸碱污染还应考虑到它的操作方便性，本装置选用了台湾生产的舞台美术使用的发烟器。

5）发烟排管的设计。由于舞台美术用发烟器喷出的是紊流烟团，显然这是不符合横流风机入口层流烟流的要求。因此必须设计发烟器末端发烟排管并将其放置在横流风机入口前方的适当位置，使进入横流风机的烟流为细而长的烟丝，这样烟谱图才能真正反映风机系统的流场情况。

6）辅助风机系统。流场显示装置的末端为一个流量可以调节的辅助风机系统，以保持风机出口处的压力为环境大气压（空调器室内机组的正常工况）。

3 横流风机流量、噪声同步实验装置的研制

它与流场显示装置一样，也是供横流风机流场和声场综合研究用的实验装置。两者所不同的是流场显示装置所提供的烟谱图仅能预测横流风机的通风性能和噪声产生机制（如涡-声换能、旋涡阻力损耗等），而不能反应横流风机在给定转速下的实际流量和噪声水平。因此有必要研制横流风机流量、噪

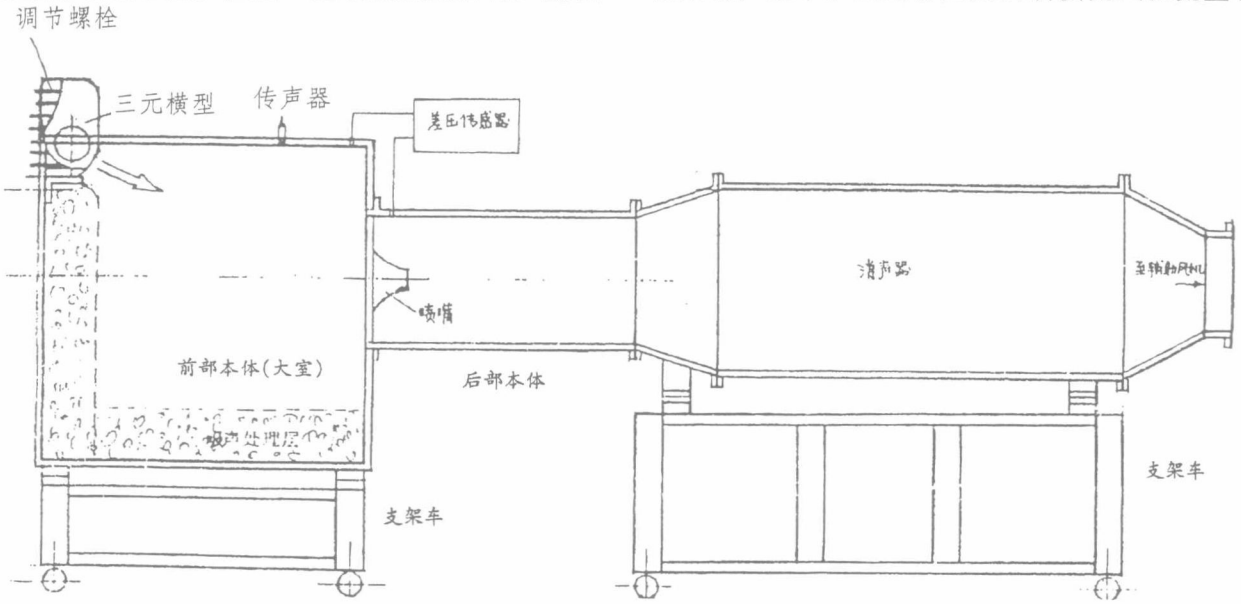

图 2 流量、噪声同步实验装置

声同步实验装置。本装置由三元模型(或成品原型)、装置本体以及流量、噪声同步分析系统组成(图2)。关于该装置的研制主要作了如下考虑:

1) 三元模型的功能设计。与二元模型类似,可以方便地调节风轮同蜗舌的间距及蜗壳的线型,以便实时对不同结构参数下的流量和噪声进行同步评估;

2) 噪声测量用装置前体的设计。为了获得横流风机的噪声数据,本装置的前体为一个较大的消声大室,大室的侧壁和底部均内敷200mm的吸声材料以消除大室中声波的反射和混响。

3) 流量测量用装置后体的设计。本装置采用节流流量法测量横流风机的流量,其节流喷管及前体和后体的尺寸参照了GB1236-85通风机机械空气动力学试验[2]和GB/T7725-1996国标[3]的相关标准。

4) 末端辅助风机方面的考虑。辅助风机的流量应与横流风机的流量相匹配,其流量采用交流变频器,根据不同横流风机的流量实时调节,以保证前体大室内的静压为当地大气压,即保证三元模型在前体大室内与在房间内的工况相同。另外,辅助风机噪声的前传会影响大室内的噪声测量数据,因此在辅助风机的前后加了进口与出口消声器。

5) 流量、噪声同步测试系统。该测量系统是以HKC-8500工控机为中心的数据采集及实时分析系统,它主要用于测量空调器用风机在给定转速和大气压下的流量、所耗功率、效率及其相对应的噪声。

4 结论

通过本装置的研制得出如下结论:

1) 该流场显示装置和流量、噪声同步实验装置目前已用于空调器新产品的开发,经试验已达到了预期的效果。

2) 由于国内对空调器的自行设计才刚起步,这种经济实用的装置比较容易推广使用。它是研究空调器通风性能和噪声水平的有效的辅助手段。

3) 该装置对今后开发轴流风机、离心风机和斜流风机流量、噪声同步实验装置具有重要的参考价值。

参考文献:

[1] Neise,W., 离心风机降噪方法述评[J]. Journal of Engineering for Industy Vol.104,151-161,1962.
[2] GB/1236-85.通风机空气动力性能试验方法[S].
[3] GB/T7725-1996.房间空气调节器[S].

·动态与信息·

浙江省电力系统噪声综合治理研讨会在杭州举行

为贯彻执行江泽民主席2001年第60号令(即中华人民共和国职业病防治法),浙江省电力工业局于2001年11月30日在杭州召开了所属各发电厂、电力公司、研究所等23个单位50名代表参加的噪声综合治理研讨会。省电力局和省电力试验研究所首先介绍了对浙江省16个发电厂噪声普查及听力保护调查情况,监测了323个岗位,2700个测点,取得了大量第一手资料。发电厂噪声源颇多,等效声级超过90dB(A)的噪声源有磨煤机、给水泵、送风机、励磁机、汽轮机、空压机和循环泵等。每工作日8小时暴露于等效声级大于等于85dB(L_{Aeg}≥85dB)岗位有149个,占被调查岗位的46%。电厂噪声直接影响到操作者的身心健康,已引起各级领导的重视,噪声性耳聋是职业病之一。国家电力系统"十五"规划明确指出,作业场所噪声合格率(L_{Aeg8}≥85dB)要达到80%以上。在研讨会上上海第九设计研究院吕玉恒高级工程师介绍了电厂磨煤机等噪声治理的实践,各厂交流了噪声治理情况,省电力局布置了下阶段工作安排。

(中国船舶工业第九设计研究院　吕玉恒　2001.12.1报导)

第 34 卷第 2 期
2002 年 4 月

南 京 航 空 航 天 大 学 学 报
Journal of Nanjing University of Aeronautics & Astronautics

Vol. 34 No. 2
Apr. 2002

文章编号:1005-2615(2002)02-0173-05

流动诱导空腔振荡预测方法的改进

田 春 张 强
(南京航空航天大学航空宇航学院 南京,210016)
李 青
(西安飞机设计研究所 西安,710089)

摘要 详细地阐述了流动诱导空腔振荡的机理,并对小尺寸空腔(长深比 $L/D=4$)做了反复的实验。基于本文的实验结果和国外飞机弹舱噪声的飞行数据及空腔的风洞实验数据,并结合流动诱导空腔振荡的机理合理改进了预测流动诱导空腔振荡各阶模态的频率方程,以及预测自由剪切层自激振荡第一阶和第三阶模态的 1/3 倍频程声压级的工程算法,结果表明,采用改进后的计算方法对流动诱导空腔振荡噪声的预测具有较高的精度,并能用于工程计算。

关键词:噪声预测;空腔;压力振荡
中图分类号:V43.28 **文献标识码**:A

引 言

鉴于空腔流动涉及到流体力学中非定常分离流、涡动力学、自由剪切层的不稳定性、紊流剪切层中相干结构(即拟序结构)、声与流动的相互作用等许多基本的前沿问题,另外,实际中如飞行器武器舱内高达 170 dB 的脉动声压级所致的附近结构的疲劳、振动和舱内武器系统的电子设备的损坏[1~3],以及跨音速风洞的开缝(孔)壁产生的噪声所致的风洞流场品质的下降[4,5]均与流动诱导空腔振荡有关。因此,国际上对流动空腔振荡的研究高度重视。从 50 年代起,就有人对空腔流动压力振荡、声辐射进行了实验研究[6,7],六七十年代后,实验文献大量涌现[8,9],同时出现了对流动的机制、振荡预估、噪声预估等的理论探讨以及振荡的抑制技术研究,出现了相关的理论分析方面的文献[1,2]。但遗憾的是各种工程预估的精度较低,无论是共振模态频率的预估还是模态频率 1/3 倍频程声压级的估算都存在着较大误差,所以有必要对工程预算中的半径验公式作进一步的改进和发展。本文通过对 $L/D=4$(L 为空腔长度,选为 0.2 m;D 为空腔深度,0.05 m)开式小尺寸空腔的大量实验,并结合国外大量的实验数据对 Rossitor 频率方程[9],Smith 和 Shaw 发展的自由剪切层自激振荡模态的 1/3 倍频程的压力脉动的预测方法[10]进行了改进,并作了实验验证,表明这一改进对流动空腔诱导噪声的预测具有重要意义。

1 流动空腔振荡的机理

从流体力学的观点考虑,流体流动在腔口前缘分离,自由剪切层内不稳定波随流动向下游发展,然后与腔后固壁相撞(通常是周期性的)产生扰动波,扰动波再以空气动力学或声学的形式传回到腔口前缘的流动分离区,使得自由剪切层不稳定波与反馈的扰动波之间相互激励、相互增强,导致空腔内流动以一族特定的频率产生很大的压力振荡并导致强烈的噪声(见图 1)。在大部分流速范围内空腔流都会发生振荡。文[11]根据振荡中所含耦合作用的类型,把它们分成如下三种形式:流体间流体动力学相互作用、流体-声学模态共振相互作用及

收稿日期:2001-04-20;**修订日期**:2001-11-25
作者简介:田 春,女,硕士研究生,1977 年 5 月生;张 强,男,副教授,1958 年 12 月生;李 青,男,高级工程师,1964 年 4 月生。

流体-弹性相互作用。很多情况下，在空腔振荡中可能同时存在上面的几种相互作用形式。一般说来，自由剪切层的自激振荡在很宽的速度范围内都存在，只是低速时，振荡较弱。因此，本文只考虑第一种形式。

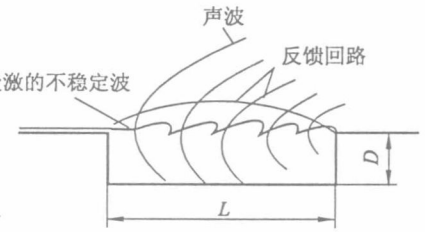

图1 典型空腔剪切层自激振荡的反馈回路

大量文献研究表明，影响空腔振荡的最主要参数是空腔的长度 L 和深度 D 的比值，根据 Sarohia 的准则[12]，通常 $L/D>1$ 时称为浅腔，$L/D<1$ 时称为深腔。浅腔流动主要受剪切层特性的影响。如果腔口剪切层再附着在空腔后壁板或更下游处，则称为“开式空腔流”(这是本文重点讨论的类型)，当 L/D 很大时，剪切层在腔的底板上再附着，则称为“闭式空腔流”，并在后壁之前的底板上产生再次分离流，介于这两者之间的称为“过渡型空腔流”。

2 流动诱导空腔振荡噪声预测方法的改进

2.1 流动诱导空腔振荡模态频率方程的改进

对开式空腔流动，文[8]提出了一个简单的涡运流声反馈模型，把腔口剪切层看作由上游腔前缘脱落的一系列涡组成，以一定的速度向下游运动，涡与腔后壁台阶碰撞，产生扰动波并向上游传播(以声速传播)，当这一扰动波反馈到前壁面时，在前缘处会激发出新的涡脱落，特别是当流场涡与反馈声波组成的反馈回路满足一定的相位关系时，流动将出现自持振荡。设涡脱落运动的波长为 λ_v，腔内由后缘碰撞产生的反馈声波波长为 λ_c，假定涡脱落的频率与由此涡碰撞后缘产生的反馈声波的频率相同，则有

$$f=\frac{K_vU_\infty}{\lambda_v}=\frac{c_\infty}{\lambda_c} \tag{1}$$

式中：K_vU_∞ 为涡运流速度；一般地，$K_v=0.57$；U_∞ 为自由流速度；c_∞ 为声速。当振荡产生时，上述反馈系统必须满足下述相位关系

$$2\pi\frac{L}{\lambda_v}+2\pi\frac{L}{\lambda_c}+2\pi\alpha=2\pi n$$

或

$$2\pi L\left(\frac{1}{\lambda_v}+\frac{1}{\lambda_c}\right)=2\pi(n-\alpha)\quad n=1,2,3,\cdots \tag{2}$$

其中第一项为涡脱落后从前缘运流至后缘的相位，第二项为反馈声波从后缘至前缘的相位，第三项为声波到达上游时与随后的涡脱落之间的相位滞后(令为 $2\pi\alpha$)。考虑到 $f=K_vU_\infty/\lambda_v=c_\infty/\lambda_c$，则可能发生振荡的无量纲频率为

$$S_n=\frac{f_nL}{U_\infty}=\frac{n-\alpha}{M_\infty+\frac{1}{K_v}}\qquad n=1,2,3 \tag{3}$$

这就是 Rossiter 提出的空腔振荡的频率方程。式中 S_n 和 f_n 是振荡的 Strouhal 数和频率，L 为空腔长度，$M_\infty=U_\infty/c_\infty$，$n$ 为正整数，对应于相位耦合的整波长数。α 和 K_v 是由实验确定的常数，其中 α 与声波到达上游时与随后的涡脱落之间的时间滞后有关，K_v 与涡运流速度与自由流速度的比值有关。文[8]指出，预测浅腔($L/D\geqslant2$)的振荡频率时 $\alpha=0.25$，$K_v=0.57$。后来 Heller 等提出向上游的扰动声波传播速度应当是空腔内的当地声速[9]，因此振荡的无量纲频率方程便改写为

$$S_n=\frac{f_nL}{U_\infty}=\frac{n-\alpha}{M_\infty/\left(1+\frac{\gamma-1}{2}M_\infty{}^2\right)^{\frac{1}{2}}+1/K_v}\qquad n=1,2,3 \tag{4}$$

式中：γ 为空气的比热比，取为 1.4。

本文在细致分析流动空腔振荡产生机制的基础上，提出当 $M_\infty<1$ 时，α 并非是一个定值，而是随 M_∞ 而变的函数。由国外大量实验数据(如图2所示)，确定 α 应修改为

$$\alpha=0.25\times(1-0.35\times10^{(0.8-M_\infty)}) \tag{5}$$

这样经本文改进后的无量纲频率 Strouhal 数($S_n=f_nL/U_\infty$)便为

$$S_n=\frac{f_nL}{U_\infty}=\frac{n-0.25\times(1-0.35\times10^{(0.8-M_\infty)})}{M_\infty/(1+0.2M_\infty{}^2)^{1/2}+1.75}\qquad n=1,2,3 \tag{6}$$

从而空腔振荡的共振频率为

$$f_n=\frac{U_\infty}{L}\cdot\frac{n-0.25\times(1-0.35\times10^{(0.8-M_\infty)})}{M_\infty(1+0.2M_\infty{}^2)^{\frac{1}{2}}+1.75} \tag{7}$$

按方程(4,6)计算的无量纲频率 S_n 与 M_∞ 的关系分别为图2中的实线和虚线，同时图2也给出了文[1]的四组实验数据及本文的实验数据。由于本文是小尺寸空腔的实验数据，第1,5阶模态不明显，